# OXIDATION EFFECTS ON THE OPTICAL CONSTANTS OF HEAVY

# METALS IN THE EXTREME ULTRAVIOLET

by

Amy Grigg

Submitted to Brigham Young University in partial fulfillment

of graduation requirements for University Honors

Department of Physics and Astronomy

June 2007

Advisor: R. Steven Turley          Honors Dean: Representative?

Signature: _____          Signature: _____

BRIGHAM YOUNG UNIVERSITY

DEPARTMENT APPROVAL

of a senior thesis submitted by

Amy Grigg

This thesis has been reviewed by the research advisor, research coordinator, and department chair and has been found to be satisfactory.

_____      _____
Date                               R. Steven Turley, Advisor

_____      _____
Date                               Eric Hintz, Research Coordinator

_____      _____
Date                               Scott Sommerfeldt, Chair

ABSTRACT


OXIDATION EFFECTS ON THE OPTICAL CONSTANTS OF HEAVY

METALS IN THE EXTREME ULTRAVIOLET

Amy Grigg

Department of Physics and Astronomy

Bachelor of Science

This thesis examines a method that takes oxidation gradients into consideration when determining optical constants from reflectance and transmission measurements. The oxidation gradients were measured by two techniques using x-ray photoelectron spectroscopy: sputtering, where data are taken at various depths in the sample after removing the surface by sputtering; and variable angle scans, where depth information is obtained by placing the detector at several angles. X-ray photoelectron spectroscopy sputtering was found to give better results for our purposes. This method resulted in very good fits of theoretical data.

ACKNOWLEDGMENTS

# Contents

# List of Figures

# Chapter 1

# Introduction

## 1.1  Principle applications of extreme ultraviolet technology

The extreme ultraviolet spectrum of light (10-100 nm) has become increasingly important to technology. Applications include photolithography, medical microscopes and space-based astronomy.

Photolithography is used in integrated circuits, particularly computer chips. The technological world, in the attempt to increase computer speed and decrease computer size, is preparing to switch to the use of extreme ultraviolet lithography. The short wavelengths of extreme ultraviolet (EUV) light allow for the creation of smaller images. Through the use of EUV lithography, a 10-fold increase in computer chip speed and 1,000-fold increase of memory storage may be achieved [1].

EUV technology also has applications in medicine. Current scanning electron microscopes are an impressive tool, but samples often require extensive preparation. The microscope slides can require metal coating and chemical treatment that significantly damage organic samples. EUV microscope samples require less preparation,

allowing scientists to view cells in a more natural environment [2].

Another application of EUV technology is space-based astronomy. The use of this technology in telescopes allows astronomers to view light produced deep within the surfaces of stars. EUV studies of stars must be conducted in space because EUV light is absorbed in the earth's atmosphere. Thus, the study of EUV light in astronomy is a relatively new field, allowing for the study of astronomical phenomenon never before accessible.

## 1.2 Past research

Unfortunately, the optical constants of materials in the EUV spectrum are not well known. The term "optical constants" refers to the complex index of refraction, $\mathcal{N} = 1 - \delta + i\beta$. The BYU Thin-Films Research Group has devoted much effort to determining EUV optical constants for applications including space-based astronomy. For example, we designed and constructed thorium dioxide mirrors for imaging singly ionized helium trapped in Venus's magnetic field (European Space Agency's Venus Express). Uranium had been the focus of study by the BYU Thin-Films Group, but was abandoned when the state of oxidation proved to be too uncontrollable for uranium to be a useful single-layer reflector. More recent studies have focused on thorium and thorium dioxide.

Thorium is an element of interest for many reasons. It only has one oxidation state, $ThO_2$. This is convenient because it allows for more control over the molecular state of the sample. Oxidation cannot be prevented, but a better understanding of the extent of oxidation allows for more accurate determination of optical constants based on physical measurements. Also, thorium is remarkably stable. It has the highest melting point of any known oxide at 2200 K, making it highly versatile.
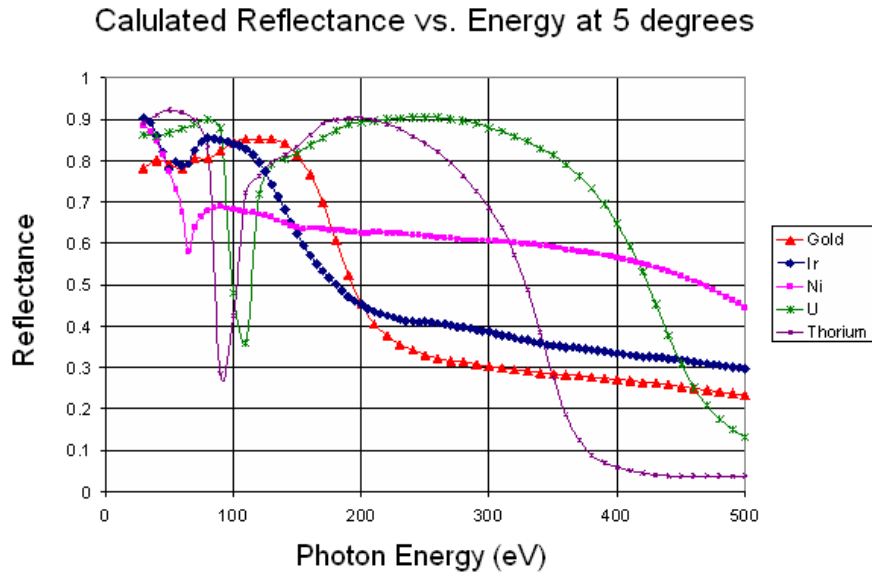
Figure 1.1: Calculated reflectance of several elements of interest in the EUV. Thorium shows high reflectance between 20-85 and 110-300 eV.

Calculations show that both thorium and thorium dioxide are good reflectors of EUV light. Fig. 1.1 is a graph of the calculated reflectance of thorium and several other elements of interest in the EUV [3].

## 1.3   Problem of oxidation

Because of the high absorption of materials in the EUV, reflection and transmission data must be obtained in vacuum with extremely thin samples. Oxidation is often negligible in the visual spectrum due to the transparency of most oxides and the relatively thin layer of oxide. In the EUV, however, oxidation has a significant effect on the optical constants of samples, as oxides are opaque in the EUV and can make up a large fraction of the sample composition. The interface between the oxide and the sample itself is particularly important in modeling the sample to determine optical

constants. The reflectivity of the sample differs greatly between an abrupt interface and one that varies smoothly. The oxidation gradient of the material must be well determined experimentally in order to accurately determine the optical constants of the materials under study.

In this study, I used X-ray Photoelectron Spectroscopy (XPS) to determine the uniformity of thin-film samples and to obtain models of oxidation as a function of depth. There are two methods of accomplishing this with XPS: sputtering, where data are taken at various depths in the sample after removing the surface by sputtering; and variable angle scans, where depth information is obtained by placing the detector at several angles. For our samples, I found sputtering to be the best method for determining oxidation gradients. I also wrote a data-fitting program that takes into account the measured oxidation gradient in determining optical constants based on reflectance/transmission data.

# Chapter 2

# Experiment

## 2.1   Molecular composition

X-ray Photoelectron Spectroscopy (XPS) is used to examine surface molecular com-
position.  XPS must be combined with depth profiling methods in order to obtain
information about depth. Our main purposes for utilizing XPS are to determine the
depth of the thorium dioxide layer, to understand how the composition changes with
depth, and to obtain an expression for oxidation as a function of depth.

XPS is based on Einstein's photoelectric effect.  X rays from a Cu K-$\alpha$ source
strike the sample, causing electrons from various depths in the sample to be emitted.
A magnetic field deflects the electron paths in an analyzer, where the electrons strike
a sensor wall.  The kinetic energy of electrons leaving the sample is inferred from
the final positions of the electrons. Fig. 2.1 depicts this process.  The energy of the
electron in the sample is then calculated using the equation, $\phi = h\nu - K_{max}$, where $\phi$ is
the minimum energy required to remove the electron from the sample (made up of the
binding energy of the electron as well as the energy of the molecular binding within
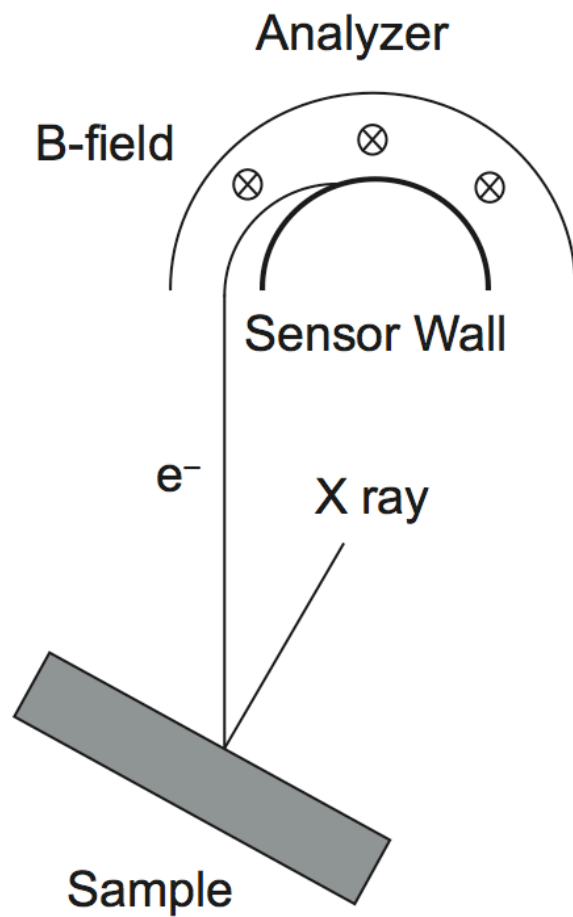the sample), $h\nu$ is the energy of an incident photon, and $K_{max}$ is the maximum kinetic

Figure 2.1: An incident photon is absorbed by and an electron is ejected from the sample, which then goes into the analyzer.
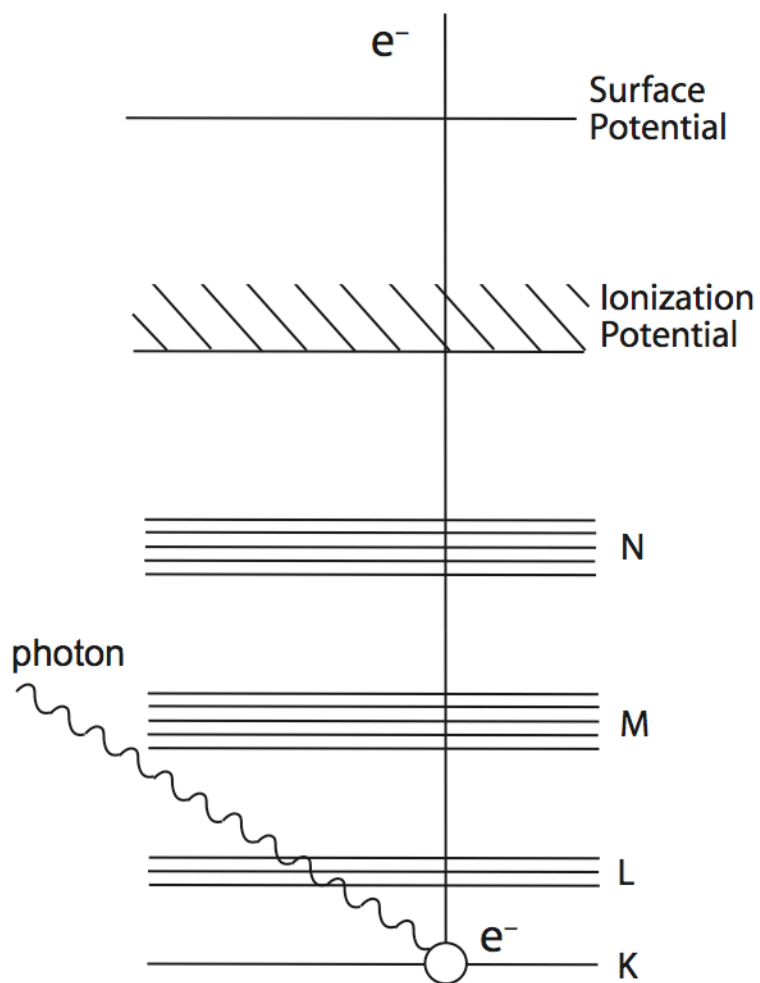
Figure 2.2: An incident photon with energy $h\nu$, where $h$ is Planck's constant and $\nu$ is frequency, ejects electron $e^-$ from the K shell of an atom.

energy of the ejected electrons. Fig. 2.2 is a schematic of the different potentials that make up $\phi$.

The number $N$ of electrons hitting the detector is given by

$$N = nf\sigma\theta\gamma\lambda AT\,, \tag{2.1}$$

where $n$ is the density of the element in the sample, $f$ is the x-ray flux in photons per unit area, $\sigma$ is the photoelectric cross section, $\theta$ is the angular efficiency factor, $\gamma$ is the efficiency for the formation of photoelectrons, $\lambda$ is the mean free path of the photoelectrons, $A$ is the area hit by the x-ray beam, and $T$ is the detector efficiency. All of these components, excluding $N$ and $n$, make up the relative atomic factor $S$. Eq. (2.1) is written as

$$N = n \cdot S\,. \tag{2.2}$$

Relative elemental composition may be determined using

$$\frac{n_1}{n_2} = \frac{N_1 \cdot S_2}{N_2 \cdot S_1}\,. \tag{2.3}$$

Eqs. (2.1)–(2.3) are necessary for deducing the elemental percentages of the data presented in Chapter 3.

XPS yields a graph, called a survey scan, of the number of electrons detected versus the binding energy in electron volts (eV). Some electrons collide or scatter on the way to the detector and consequently lose energy. These electrons form the flat region between peaks visible in Fig. 2.3. In the graph, each peak corresponds to the transition level of an element. The relative elemental concentrations can be deduced from the integrated counts in these peaks by using Eq. (2.3). There are several peaks visible in this Si sample (Fig. 2.3): F at 680 eV, O at 530 eV, C at 280 eV, and Si at 105 eV and 180 eV. These are some common contaminants that appear after the sample has been cleaned (F) or exposed to air (O and C). Note that the formulas
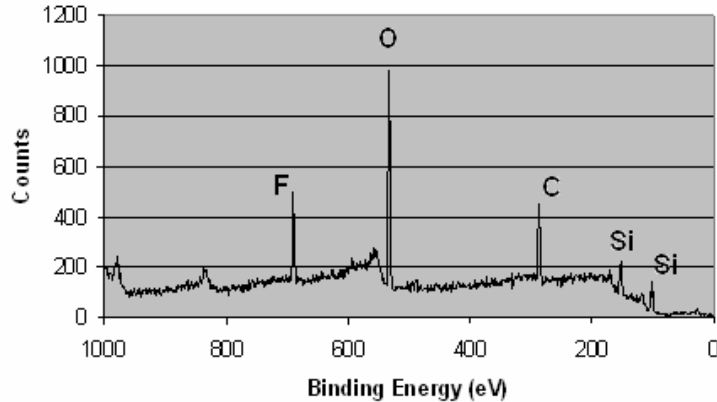
Figure 2.3: Survey scan of a hydrocarbon-contaminated silicon wafer. Each peak corresponds to an element: F at 680 eV, O at 530 eV, C at 280 eV, and Si at 105 eV and 180 eV.

for $S$, the $S$ values and information about peak positions in this study were taken from the Handbook of X-ray Photoelectron Spectroscopy [4].

In addition to elemental percentage, relative elemental peak shifts are used to determine the molecular state of the sample. Element peak positions shift to higher or lower energy levels when the atoms are bound to other elements. This allows us to determine the specific type of binding in the sample. The shifts are usually between 2 and 7 eV.

Double peaks indicate a partial state. For example, some oxygen molecules may be at one energy (530 eV) and others at a higher energy (534 eV, bound with thorium). If the sample is scanned with depth at different locations, information may be obtained about the structure of the sample oxidation. For example, some elements oxidize with a finger-like structure, which would show changes in percentages and partial peaks as the sample is scanned across the surface. Information may be obtained about this oxidation structure using XPS methods combined with depth profiling techniques.

Depth profiling is used to examine the lower levels of the sample. There are two
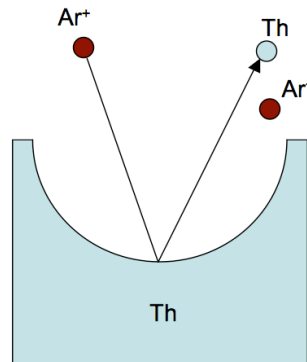
Figure 2.4: Sputtering is used to remove layers and obtain a compositional profile with depth.
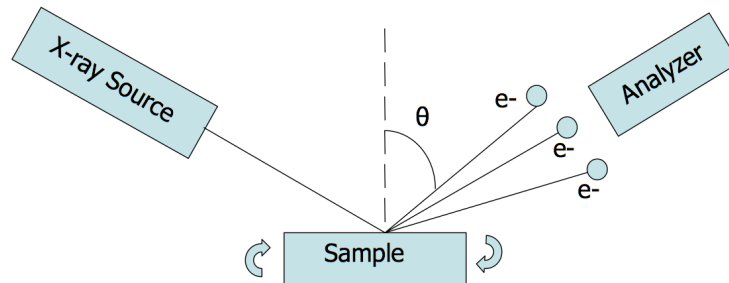


Figure 2.5: The sample is scanned at different detector angles to obtain depth information.

methods of profiling composition with depth. In the first method, a hole is made in the sample by emitting a stream of argon ions across the sample under high vacuum, a process known as sputtering. The massive argon ions, having a large kinetic energy, remove molecules from the surface of the sample. The depth at which the sample is scanned, or at which electrons are ejected and analyzed, is proportional to the density of the sample and the time spent sputtering. It can take many hours depending on the the thickness, mass and density of the sample. Fig. 2.4 depicts this process.

The second method is called angle-resolved x-ray photoelectron spectroscopy, or ARXPS. With this method, the sample is placed on a variable-angle sample holder and scanned at different detector angles while the x-ray angle is held constant. The electrons ejected from deeper in the sample can escape the surface at angles near normal, whereas the electrons from the same depth that escape at shallow angles have to travel through more material and are more likely to be absorbed. Depth information is obtained by measuring the number of emitted electrons as a function of sample angle. Fig. 2.5 depicts this process. The advantages and disadvantages of these two methods will be examined in Chapter 3.

## 2.2 Thickness

It is important to know the thickness of the film to extrapolate the thicknesses of the layers determined by XPS. There are two methods used in this study to determine the thickness of the sample. In the first method, spectroscopic ellipsometry, light at a variety of visible wavelengths and angles is shone on the sample. The resulting light is made up of several different phases depending on the interface from which it was reflected. The relative phase of the resulting light and known (or extrapolated) optical constants are used to determine the thickness of the material.

The second method for determining thickness is x-ray diffraction, where an x-ray beam is shone on the sample surface and Bragg peak positions are detected. The light reflected from each of the interfaces creates an interference pattern. The peak positions are fit to determine the thickness of the sample.

## 2.3 Reflectance and transmission

Optical constants, as defined in Section 1.2, are determined from reflectance and transmission data. [12] Data are obtained through the use of a monochromator, which utilizes a series of gratings and pinholes to isolate a single wavelength from a hollow-cathode source. This monochromatic light is then reflected off the surface in question and detected at various angles. The monochromator at BYU is capable of taking measurements at selected wavelengths between 304 and 1216 angstroms. It is currently set up for reflectance measurements only, though with modification it is capable of taking transmission measurements as well.

We also take reflectance and transmission measurements with synchotron radiation at the Advanced Light Source (ALS) in Berkeley, CA. The ALS offers a broader choice of photon energies, gratings, and filters. It also offers a continuous wavelength range, and a setup conducive to taking transmission measurements. The reflectance/transmission data are then fit to the formulas found in Chapter 4.

# Chapter 3

# Results

## 3.1   Sample preparation

All sample films are deposited on silicon wafers via DC magnetron sputtering in an argon plasma. Multiple samples are made in the same deposition run. The extra samples are called witness samples and are used for thickness and composition analysis, so as not to damage the sample used to obtain reflectance and transmission measurements. Note that there are two types of sputtering used in this study: XPS sputtering, where layers are sputtered off to obtain information with depth, and DC magnetron sputtering where atoms are sputtered off a target and deposited on a silicon wafer. The base vacuum pressure in the sample deposition chamber is below $3 \times 10^{-6}$ torr. The base vacuum pressure in the XPS chamber is below $1 \times 10^{-8}$ torr. Reactively sputtered thorium dioxide is made in addition to thorium for this study, meaning that oxygen was introduced into the chamber during sputtering to create a uniform oxide.
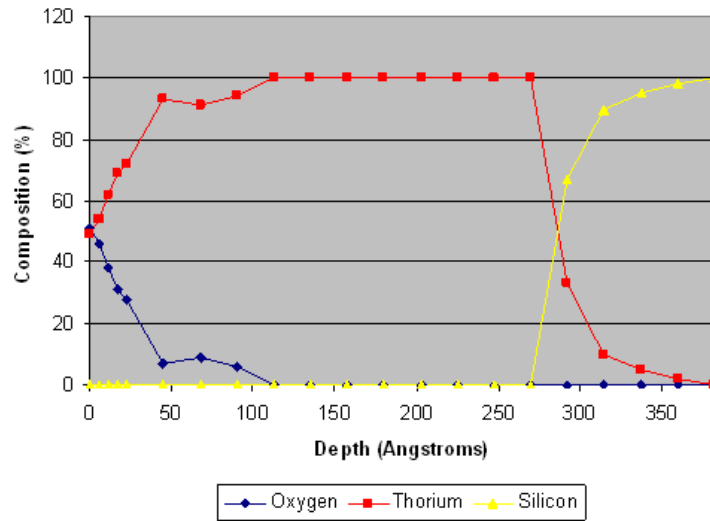
Figure 3.1: Depth profile of Thorium. The surface of the sample has oxidized nearly linearly for about 80 angstroms.

## 3.2 Sample composition

Fig. 3.1 is a graph of the depth profile done by XPS sputtering of a naturally oxidized thorium sample, obtained a few hours after the sample was produced. The graph displays the elemental percentage with depth. The sample appears to be oxidized nearly linearly for about 80 angstroms. However, this is not the true interface since we can detect electrons produced at depths of up to 50 angstroms into the sample. This is also why the measured thorium-silicon interface is not abrupt.

The probability $P$ of an electron escaping from the sample is proportional to the differential probability $\partial P$ of an electron within a given depth $\partial x$ escaping.

$$P = -\alpha \frac{\partial P}{\partial x} \tag{3.1}$$

Here, $x$ is the depth of the electron in the sample and $\alpha$ is a constant. If we solve this differential equation by separating variables, we obtain
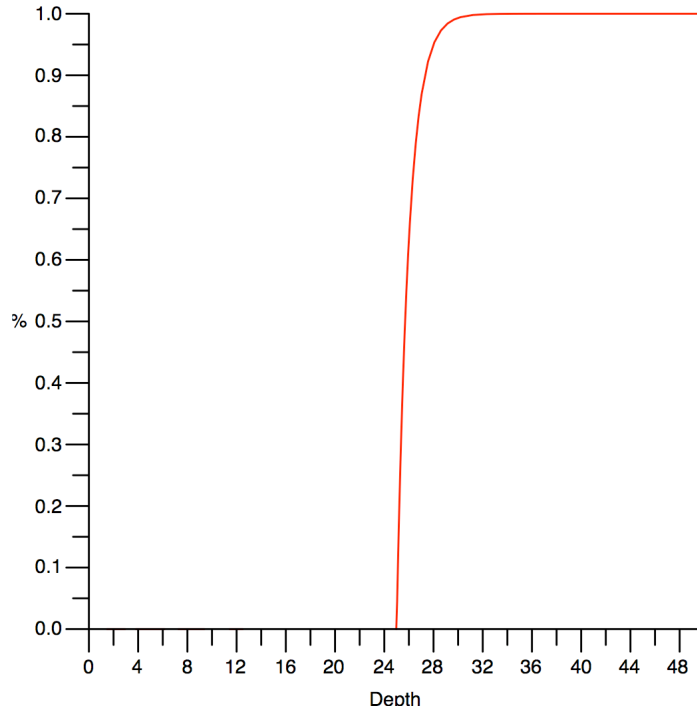
Figure 3.2: This is how an abrupt interface would appear if examined via XPS.

$$P(x) = ke^{-\alpha x} . \tag{3.2}$$

The probability of an electron escaping the sample is an exponential function of the depth of the electron in the sample. Because of this, we expect to see an exponential curve when the interface is abrupt and some combination of the shape of the interface and an exponential when it is not abrupt.

To determine the relationship of elemental percentage with depth, we must take the convolution of $P(x)$ and the function $f(x)$ that describes the depth profile.

$$Perc = \int_0^\infty f(x')P(x - x')dx' \tag{3.3}$$

Fig. 3.2 is a graph obtained using Eq. (3.3) of how an abrupt silicon interface would appear if examined via XPS. This is very similar to the silicon interface in
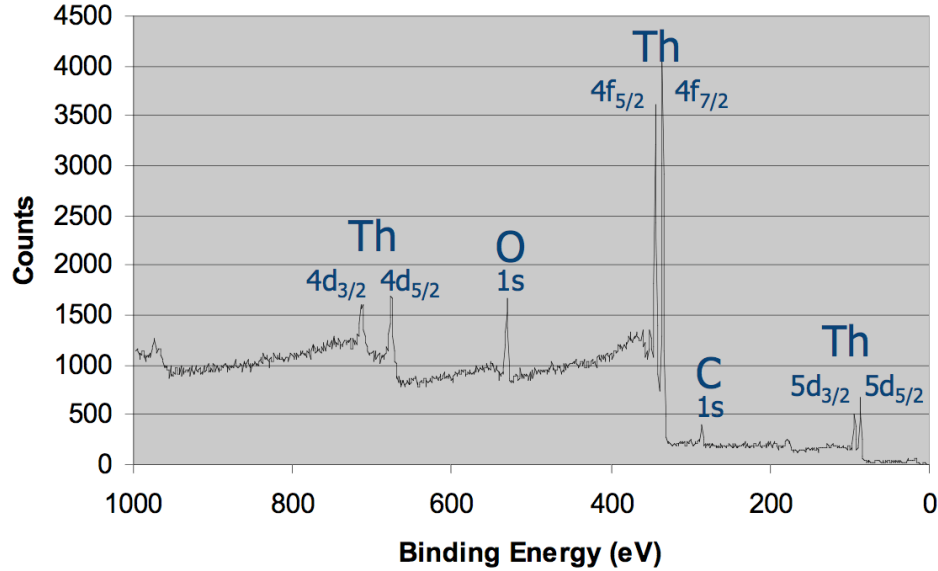
Figure 3.3: Survey scan of thorium dioxide

Fig. 3.1. Since thorium and silicon do not generally bond, this interface is expected to be abrupt. The XPS results agree with this hypothesis. The constant $\alpha$ may now be obtained by fitting the thorium-silicon interface to the equation obtained for the ideal interface. To determine the shape of the real interface based on the measured interface, we must apply the Convolution Theorem (the convolution of two functions is equal to the product of their Fourier transforms), given by

$$\int_0^\infty f(x - x')P(x')dx' = \mathcal{F}(f(x))\mathcal{F}(P(x)), \tag{3.4}$$

where $\int_0^\infty f(x - x')P(x')dx'$ is the measured interface. The real interface is given by

$$f(x) = \mathcal{F}\left(\frac{\int_0^\infty f(x - x')P(x')dx'}{\mathcal{F}^{-1}(P(x))}\right). \tag{3.5}$$

Thorium is found to oxidize rapidly when exposed to air. Samples must be left under vacuum when not in use. Reflection and transmission measurements must be taken within an hour or two after deposition if the sample is exposed to air.

Fig. 3.3 is a survey scan of thorium dioxide which indicates the peak locations. Figs. 3.4 and 3.5 are survey scans focused on the thorium $4f$ peaks. Fig. 3.4 is a graph of the thorium 4f peaks on the surface of the sample. Fig. 3.5 is a graph of the thorium peaks lower in the sample after the oxide layer has been sputtered off. The change in peak shape is due to oxygen bonding on the surface. The peaks are thinner in the presence of oxygen. There is also a slight shift in the energy level. In this case, the thorium peaks are found to shift 2 eV higher in the presence of oxygen. This shows that the oxygen is bound to the thorium on the surface, and not bound to surface contaminants.
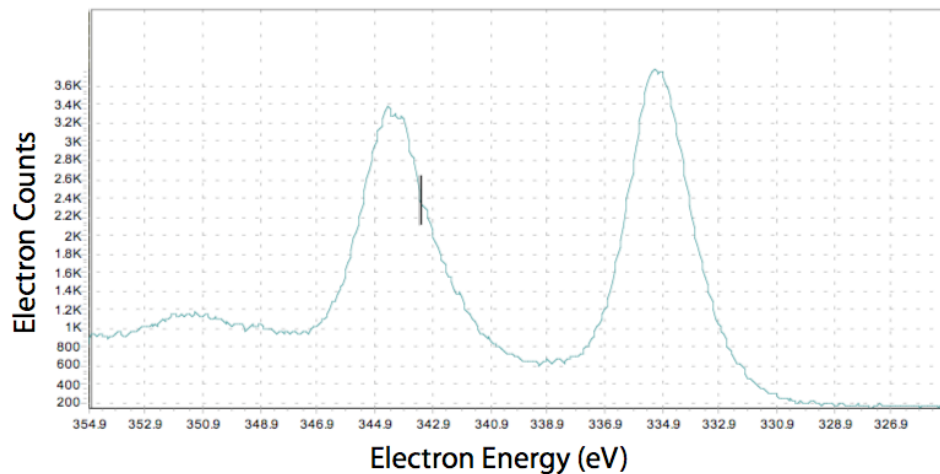


Figure 3.4: Thorium peaks on surface

Although thorium is not generally considered to oxidize, the results show that thorium thin films do oxidize enough to alter the optical constants of our sample. Comparing the overall XPS scans with thickness measurements taken by x-ray diffraction and assuming linear correlation between depth of XPS sputtering and sputter time, the thorium oxide layer extends about 80 angstroms down into the sample. This is an approximation, however, because technically the different masses and densities of the thorium dioxide and thorium layers should make it sputter through some of the
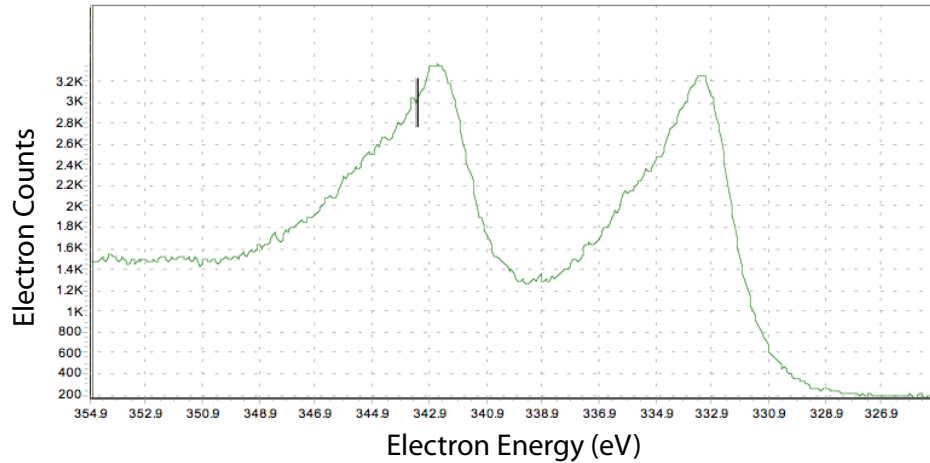
Figure 3.5: Thorium peaks after oxygen is gone

sample more quickly than other parts. The mass and density of thorium and thorium dioxide are close enough that the approximation works well. About 10 % of the sample is oxidized. Similar results were seen with witness samples, and other samples of this age. These expressions for oxidation may now be used to more effectively mathematically model and study the reflectance of thorium.

Because of the rapid oxidation rate of thorium samples, thorium dioxide samples were reactively sputtered for analysis (See Section 3.1 for definition). This does not yield the optical constants for thorium, but for thorium dioxide, which is itself a material of interest with high reflectance in the extreme ultraviolet range. Fig. 3.6 is a graph of the calculated reflectance of thorium and thorium dioxide in the EUV range [3].

Figs. 3.7 and 3.8 show that reactively sputtered thorium dioxide is found to be a fairly uniform oxide. The percentages of thorium and oxygen stay between 62 to 66 % thorium and 38 to 34 % oxygen, indicating the proper ratio of two to one for a fairly uniform thorium dioxide. Peak shifts indicate that the material is thorium dioxide as well. Near the surface of the sample there was a slightly higher percentage of oxygen,

**Calculated Reflectance (45 degrees)**
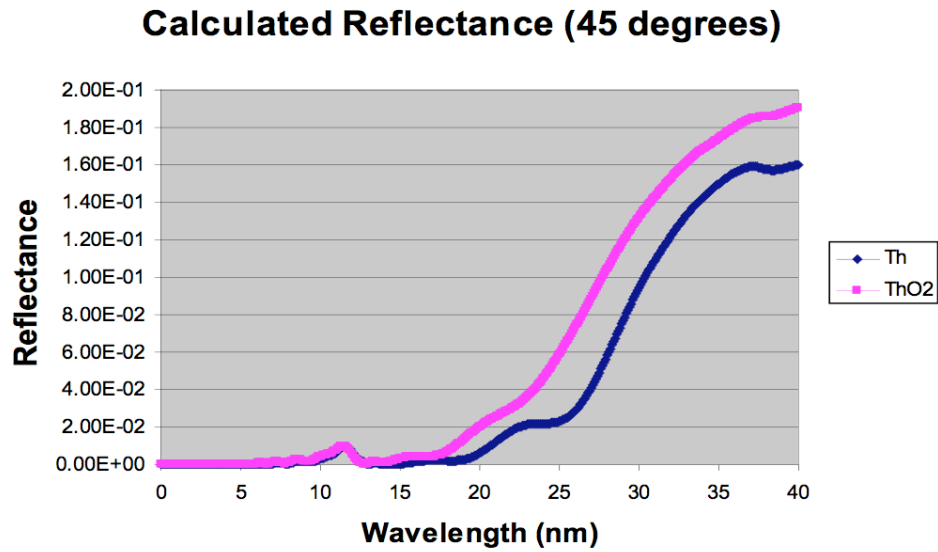


Figure 3.6: Calculated reflectance of thorium and thorium dioxide at 45 degrees
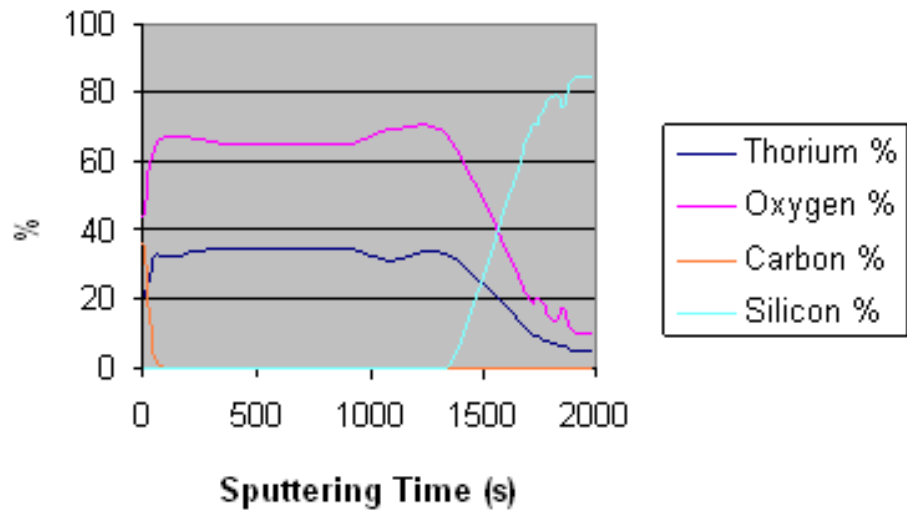


Figure 3.7: Depth profile of thorium dioxide. Reactively sputtered thorium dioxide is found to be quite uniform.
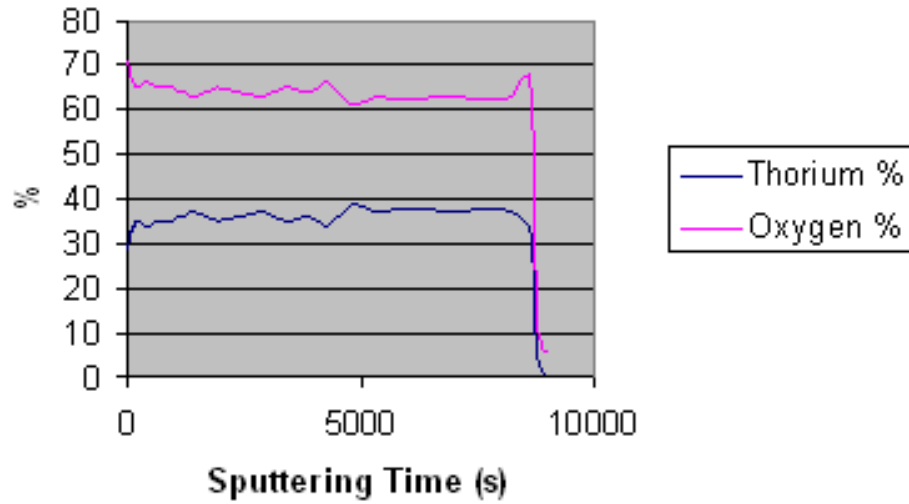
Figure 3.8: Uniform thorium dioxide composition

indicating additional oxygen contamination due to air exposure. This change in oxidation is slight, but may also be taken into account when fitting reflectance/transmission data using the same method as with thorium.

Note that the graph in Fig. 3.8 has bumps, whereas the graph in Fig. 3.7 is smooth. The computer is programmed to take various scans as it sputters. Often the more interesting features are found near the surface of the sample, so the computer is programmed to take more scans near the surface. Once the interesting features have been scanned, the computer is stopped for four or five minutes and reprogrammed to take scans less often. The graph in Fig. 3.8 is a case where this occurred, whereas the graph in Fig. 3.7 was obtained by taking continuous scans. The hikes in oxygen percentage visible in Fig. 3.8 take place at the exact times that the process was halted for several minutes to reprogram the computer. As the scans took place in high vacuum and the sample was not left long enough for the little oxygen in the chamber to be deposited, it is likely that the hikes in oxygen are due to the diffusion of oxygen molecules from lower in the sample. This feature was seen in both reactively

sputtered thorium dioxide and naturally oxidized thorium.

Results indicate that thorium does oxidize rapidly enough to change the optical constants of the samples when exposed to air. This suggests that each sample intended for reflectance/transmission measurements to determine optical constants should first be analyzed with XPS to determine the uniformity of the sample and extent of oxidation. These data may then be applied to the fitting of the reflectance/transmission measurements for more accurate determination of optical constants.

## 3.3 Sputtering vs. angle resolved XPS

The method of XPS sputtering is shown to be the best method for determining molecular composition with depth. Sputtering allows for the collection of data from the whole depth of the sample. Relative depth may be determined after the whole depth of the sample has been scanned.

There are limitations to the ARXPS depth profiling method. One is that it is a surface-sensitive technique. Although x rays penetrate more at normal angles of incidence, the signal originates from the entire x-ray path. This can smear out small features in the change of elemental composition with depth. For this same reason, it is difficult to characterize a scan depth. It is possible to obtain atomic depth resolution by fitting for many parameters at once, as was shown by Williams and Beebe in 1997 and by Brundle *et al.* in 2005 [5,6]. For our purposes, however, ARXPS is a method that is better used to determine the surface contamination and oxidation of samples, rather than to determine the depth profile.

# Chapter 4

# The Program

## 4.1   Approximating oxidation with a multilayer

Once molecular composition data are obtained, these data must be incorporated into the way the reflectance/transmission data are fit to determine optical constants. I have written a program in MATLAB that takes into account the measured oxidation in order to more accurately determine the optical constants of the material.

We have taken oxidation into account when determining optical constants in the past, but we assumed the interface to be ideal. Experiment has shown that there is a gradient between the oxide layer and the material, where the composition is a fraction thorium dioxide and a fraction thorium. So the real interface looks a little more like the interface on the left in Fig. 4.1 than the interface on the right.

The complex index of refraction, $\mathcal{N}$, is proportional to the density. Since the density is shown to vary between that of thorium dioxide and that of thorium, the interface may be approximated with a series of layers with $\mathcal{N}$ varying between the $\mathcal{N}$ for thorium dioxide and the $\mathcal{N}$ for thorium, based on the measured compositional density gradient [7]. This approximation is really a first order approximation. Jede-

Real Interface

ThO$_2$

Th

Ideal Interface

ThO$_2$

Th
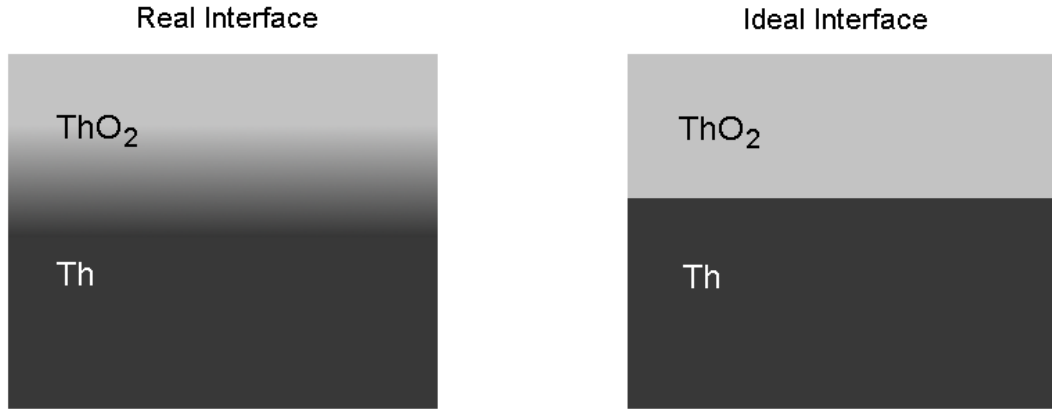
Figure 4.1: Real versus ideal interface

diah Johnson did a more complex approximation for roughness that works the same way, except with $\mathcal{N}$ varying between that of air and thorium.

## 4.2   Fresnel Coefficients

The Fresnel coefficients, $f$ and $g$ respectively, are the ratios of reflected and transmitted electric fields to the incident electric field. We use the coordinate system depicted in Fig. 4.2. The wave number $k$ is denoted by

$$k = \frac{2\pi n}{\lambda},\tag{4.1}$$

where $\lambda$ is the wavelength in vacuum, and $n$ is the index of refraction of the material. According to Snell's Law, the $y$-component of $k$ is invariant in each layer, and is given by

$$k_y = k\cos(\theta).\tag{4.2}$$

Similarly, the $z$-component of $k$ is

$$k_z = \sqrt{k^2 - k_y^2}.\tag{4.3}$$
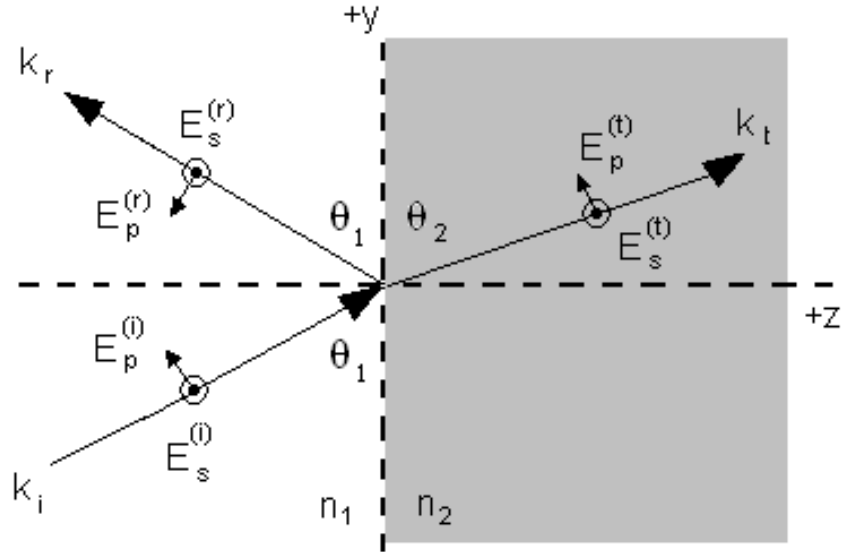
Figure 4.2: Axis of polarization

The Fresnel coefficient for reflection $f$ off the region 1 to region 2 interface for s-polarized light is [8, 9]

$$f_{12}^s = \frac{n_1 \sin(\theta_1) - n_2 \sin(\theta_2)}{n_1 \sin(\theta_1) + n_2 \sin(\theta_2)}. \tag{4.4}$$

By using a few trigonometric identities and by inserting a factor of $\frac{2\pi}{\lambda}$ into the top and bottom of the equation, we obtain a version of the Fresnel coefficient for s-polarized light in terms of the $k_z$ vector. Eq. (4.4) becomes

$$f_{12}^s = \frac{k_{z1} - k_{z2}}{k_{z1} + k_{z2}}, \tag{4.5}$$

where $k_{z1}$ is the $k_z$ vector, as defined by Eq. (4.3), in region 1 and $k_{z2}$ is the $k_z$ vector in region 2.

By the same method, all the Fresnel coefficients may be obtained in terms of $k_z$ vectors and indices of refraction $n$. The Fresnel coefficient for reflection of p-polarized

light is

$$f_{12}^p = \frac{n_2^2 k_{z1} - n_1^2 k_{z2}}{n_2^2 k_{z1} + n_1^2 k_{z2}} \,. \tag{4.6}$$

The Fresnel coefficient for transmission of s-polarized light is

$$g_{12}^s = \frac{2 k_{z1}}{k_{z1} + k_{z2}} \,, \tag{4.7}$$

and likewise for p-polarized light,

$$g_{12}^p = \frac{2 n_1 n_2 k_{z1}}{n_2^2 k_{z1} + n_1^2 k_{z2}} \,. \tag{4.8}$$

The coefficients for reflecting off of or transmitting through the region 2 to region 1 interface may be obtained by switching the 1 and 2 indices in the above coefficients. These are the forms of the Fresnel coefficients that I have used in the program.

## 4.3   Matrix Method

We take $z$ to be positive in the downward direction and label the layers accordingly, as depicted in Fig. 4.3. The beams in the $+z$ direction are denoted by $U$ ("up") and the beams in the $-z$ direction are denoted by $D$ ("down"). If $U_1^s$ is taken to be the beam at the surface of the interface between layers one and two and $U_1$ to be the beam at some distance away from the surface (which distance is half way in between the layers when there are more than two), then

$$U_1^s = U_1 c_1 \,, \tag{4.9}$$

where $c_1$ is the propagation coefficient in region one, which will be defined later. By the same reasoning, the beam coming out of the surface is

$$D_1^s = \frac{D_1}{c_1} \,. \tag{4.10}$$
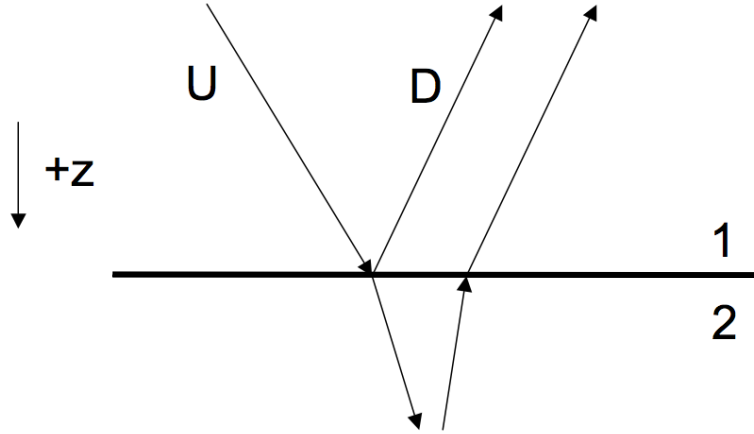
Figure 4.3: Single interface

This approach also gives

$$U_2^s = \frac{U_2}{c_2} \tag{4.11}$$

and

$$D_2^s = D_2 c_2 \,, \tag{4.12}$$

where $c_2$ is the propagation coefficient in region 2.

Next, construct equations for $D_1$ and $U_2$ based on the beam set up shown in Fig. 4.3. The downward-facing beam at the surface $D_1^s$ is made up of the beam $U_1$ after it reflects off the surface and the beam $D_2$ after it has transmitted through the region 2 to region 1 interface. This gives

$$D_1^s = f_{12} U_1^s + g_{21} D_2^s \,, \tag{4.13}$$

where $f$ and $g$ indicate the fresnel coefficients for reflection and transmission and the subscripts indicate which interface the beam is reflecting off/transmitting through.

If the beams are defined from a point at some distance from the interface, the absorption and the change in phase of the beam as it propagates through the layer

must be taken into account. This is done by adding in the propagation coefficient $c$.

$$D_1 = c_1^2 f_{12} U_1 + c_1 c_2 g_{21} D_2 \tag{4.14}$$

Also, the beam $U_2$ is made up of the transmitted beam from $U_1$ and some arbitrary beam from other possible reflective surfaces below $D_2$. This gives

$$U_2^s = g_{12} U_1^s + f_{21} D_2^s, \tag{4.15}$$

which, when defined at a point some distance from the surface, gives

$$U_2 = c_1 c_2 g_{12} U_1 + c_2^2 f_{21} D_2. \tag{4.16}$$

Now these tools are used to construct an expression for the beams above the surface in region one as a function of the beams in region two, the propagation coefficients and the fresnel coefficients of the interface. Begin by solving Eq. (4.16) for $U_1$, giving

$$U_1 = -\left(\frac{c_2 f_{21}}{c_1 g_{12}}\right) D_2 + \left(\frac{1}{c_1 c_2 g_{12}}\right) U_2. \tag{4.17}$$

Then plug this expression for $U_1$ into Eq. (4.14) and we obtain

$$D_1 = \left(c_1 c_2 g_{21} - \frac{c_1 c_2 f_{21} f_{12}}{g_{12}}\right) D_2 + \left(\frac{c_1 f_{12}}{c_2 g_{12}}\right) U_2. \tag{4.18}$$

Thus, the up and down beams in region one as a function of the up and down beams in region two are obtained.

Now combine Eq. (4.17) and Eq. (4.18) into a single matrix.

$$\begin{pmatrix} D_1 \\ U_1 \end{pmatrix} = B \begin{pmatrix} D_2 \\ U_2 \end{pmatrix} \tag{4.19}$$

The matrix $B$ is constructed that relates the beams above the surface to the beams below the surface.

$$B = \begin{pmatrix} c_1 c_2 g_{21} - \frac{c_1 c_2 f_{21} f_{12}}{g_{12}} & \frac{c_1 f_{12}}{c_2 g_{12}} \\ -\frac{c_2 f_{21}}{c_1 g_{12}} & \frac{1}{c_1 c_2 g_{12}} \end{pmatrix} \tag{4.20}$$

Vacuum

_____

1

_____

2

_____

3

_____

4

_____

5

_____

Substrate
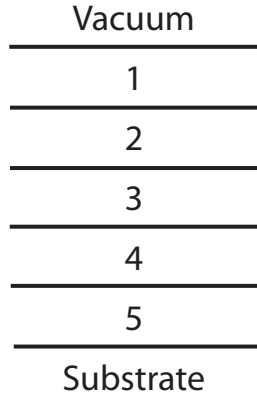
Figure 4.4: Five-layer stack

This method can be generalized for any number of interfaces. There is a characteristic matrix $B$ for every interface that relates the electric field above and below the interface. We can combine these matrices by multiplying them together in succession to obtain a matrix that characterizes the behavior of light as it travels through the entire multilayer. For example, if subscript $v$ indicates vacuum, $s$ is substrate and $T$ is total, in a six-layer mirror

$$\begin{pmatrix} D_v \\ U_v \end{pmatrix} = B_T \begin{pmatrix} D_s \\ U_s \end{pmatrix}, \tag{4.21}$$

where $B_T$ is the matrix that characterizes the entire multilayer. The matrix $B_T$ is the product of the characteristic $B$ matrices for layers 1, 2, 3, 4 and 5.

$$B_T = B_5 B_4 B_3 B_2 B_1 \tag{4.22}$$

See Fig. 4.4 for the numbering of layers. There are two such matrices $B_T$ that characterize the behavior of the light above and below the entire stack, one for s polarization and one for p polarization.

Now the total reflectance and transmission through the film is determined. Set the $D_v$ beam (the down beam in vacuum) equal to one because the amount of light

transmitted and reflected is relative to the amount of incident light. All beams are normalized to this incident beam. By definition the $U_v$ beam (the up beam in vacuum) is the light reflected from the entire multilayer which we will call $r$. There will be no $U_s$ beam (the up beam in the substrate) because at the last the last layer there won't be another interface from which the beam can reflect, so this term is set equal to zero. The $D_s$ beam (the down beam in the substrate) is the beam that has travelled all the way through the multilayer. By definition this is equal to the total transmission $t$. This yields

$$\begin{pmatrix} r \\ 1 \end{pmatrix} = B_T \begin{pmatrix} 0 \\ t \end{pmatrix}. \tag{4.23}$$

Solving this equation for $r$ and $t$ obtains

$$r = \frac{B_{12}}{B_{22}} \tag{4.24}$$

and

$$t = \frac{1}{B_{22}}, \tag{4.25}$$

where the subscripts of $B$ now indicate which matrix element of the $B_T$ matrix according to row and column.

The total reflectance $R$ is the linear combination of the magnitude squared of $r$ for s and p polarizations, weighted by the percentage of each polarization in the incident beam.

$$R = p_s |r_s|^2 + p_p |r_p|^2, \tag{4.26}$$

where $p_s$ is the percentage of light with s polarization and $p_p$ is the percentage of light with p polarization in the incident beam [9].

Thus we have constructed a matrix method for determining the optical properties reflection $r$ and transmission $t$ of a multilayer film by extending the single interface method.

## 4.4 Transmission

The total transmission of a multilayer must be treated a little differently than the reflection. The total transmission $T$ cannot be obtained like the reflection $R$ is in Eq. (4.26) because the final beam is not necessarily returning to the initial medium like reflection. Hence, a formula like

$$T = p_s|t_s|^2 + p_p|t_p|^2 \tag{4.27}$$

does not work. This derivation closely follows the work of R. Steven Turley [10].

The total transmission $T$ is linearly related to the square of $t$, but the exact relation must be determined. The correct formula is derived from the condition that energy must be conserved. The amount of light reflected, transmitted and absorbed must equal the amount of incident light. At a single interface where there is no absorbed light,

$$R + T = 1. \tag{4.28}$$

Define $\alpha$ to be the coefficient that relates $T$ to $t$.

$$T = \alpha|t|^2, \tag{4.29}$$

where, in a single layer, $t$ is the Fresnel coefficient $g$ and $r$ is the Fresnel coefficient $f$. Substituting Eqs. (4.26) and (4.29) into Eq. (4.28) obtains

$$|r|^2 + \alpha|t|^2 = 1. \tag{4.30}$$

Eqs. (4.5) and (4.7) give the coefficients for s-polarized light beginning in layer 1 and transmitting through, or reflecting off, layer 2.

$$r_s = \frac{k_{z1} - k_{z2}}{k_{z1} + k_{z2}} \tag{4.31}$$

$$t_s = \frac{2k_{z1}}{k_{z1} + k_{z2}} \tag{4.32}$$

Solving Eq. (4.30) for alpha using the $r_s$ and $t_s$ for s-polarized light yields

$$\alpha_s = \Re\left(\frac{k_{zs}}{k_{zv}}\right),\tag{4.33}$$

where $k_{zs}$ is $k$ in the exit layer and $k_{zv}$ is $k$ in the incident layer, and $\Re$ is the real part of the expression.

The same process is done for p-polarized light. Eqs. (4.6) and (4.8) give

$$r_p = \frac{n_1^2 k_{z2} - n_2^2 k_{z1}}{n_1^2 k_{z2} + n_2^2 k_{z1}}\tag{4.34}$$

$$t_p = \frac{2 n_1 n_2 k_{z1}}{n_1^2 k_{z2} + n_2^2 k_{z1}}\tag{4.35}$$

for light with p polarization. Solving Eq. (4.30) for $\alpha$ again using $r_p$ and $t_p$ yields

$$\alpha_p = \Re\left(\frac{n_v n_s^* k_{zs}}{n_s n_v^* k_{zv}}\right).\tag{4.36}$$

Combining the results for s and p polarizations yields

$$T = p_s \Re\left(\frac{k_{zs}}{k_{zv}}\right)|t_s|^2 + p_p \Re\left(\frac{n_v n_s^* k_{zs}}{n_s n_v^* k_{zv}}\right)|t_p|^2,\tag{4.37}$$

an energy-conserving equation for the total transmission $T$ of a stack.

## 4.5  Least squares fit

The program finds the most likely combination of optical constants $\delta$ and $\beta$ to have produced the measured data that is input. It uses a least squares routine, where $\chi^2$, which corresponds to the squared difference between the measured and expected values, is minimized.

$$\chi^2 = \sum_{i=1}^{N}(f(x_i) - y_i)^2,\tag{4.38}$$

where $y_i$ is the measured value and $f(x_i)$ is the expected value, computed by the matrix method with Fresnel coefficients and input $\delta$ and $\beta$ [11].

## 4.6   Simplex vs. unconstrained method

There are two methods of minimizing Eq. (4.38) that are utilized by the program. Both methods require an initial guess, or starting place for the routine to fit $\chi^2$. The first is a more robust method called the simplex routine. It chooses guesses around the initial guess and continues choosing guesses in the direction with the best results. The simplex method is used first in the program to obtain a good initial guess for the optical constants. This lowers the likelihood of obtaining a local minima, as opposed to a global minima of the $\chi^2$ function. The second method is an unconstrained method, which minimizes more quickly, but requires a more accurate initial guess. The unconstrained method minimizes more quickly because it uses information from the computed numerical gradient of the function to determine which is the best way to change the optical constants to minimize the $\chi^2$ function [11].

## 4.7   Fits

Thus, we have a program that inputs the measured reflectance or transmittance of a film and the measured oxidation gradient, and then outputs the optical constants, $\delta$ and $\beta$. The program's task is to find the most likely $\delta$ and $\beta$ to have produced the measured reflectance or transmission, based on the measured interface. It fits $\delta$ and $\beta$ by minimizing $\chi^2$, which is defined in Eq. (4.38). It uses the matrix method to compute reflectance and transmission based on many different $\delta$'s and $\beta$'s until a set is found with the least $\chi^2$.

Fig. 4.5 is an example of the fit obtained by the program. The stars are the input data points and the line is the program's fit. The input $R$ data is simulated with different amounts of random noise added. The program is quite good at fitting when the initial guess ranges for $\delta$ and $\beta$ are within 0.5.
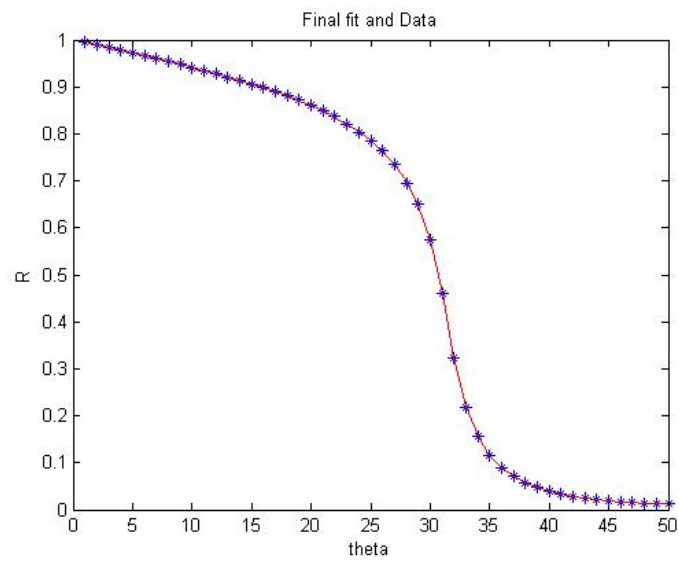
Figure 4.5: Final fit

# Chapter 5

# Conclusions

## 5.1 Thorium shows definite promise as EUV reflector

Thorium has high reflectance in the extreme ultraviolet, but, without a protective layer, may not be as useful for technological purposes. The oxidation of thorium is rapid and difficult to control when exposed to air. Reactively sputtered thorium dioxide, however, is a more stable, controllable, uniform material that may be more useful for technological applications.

## 5.2 Sputtering method vs. variable angle scan

X-ray photoelectron sputtering is shown to be the best method for determining molecular composition gradients or the uniformity of a sample with depth. Angle resolved x-ray photoelectron spectroscopy is a useful method for determining the extent of surface contamination. Both methods require deconvolution to obtain the real surface from the measured surface. The deconvolution of a sputtered depth profile is much

simpler to perform, whereas obtaining the real surface of a variable angle profile requires fitting many variables at once. The sputtering method yields information about the entire sample, regardless of thickness, whereas the variable angle profile yields composition to a depth of about 80 angstroms. If both methods are used together, however, information about the shape of the real interface from sputtering may be used to better determine the depth of the variable angle scan, and a more complete picture may be obtained. This option requires further study.

## 5.3 The program

The Matlab program determines the optical constants of a stack based on measured reflectance or transmission. The method of approximating oxidation gradients by varying n from one layer to the next yields better fits than when the layers are approximated based on an ideal interface. Future research includes making the program more robust, so the program can fit correctly even with noisy data or when the initial guess ranges aren't well known, analyzing the error in the $\delta$ and $\beta$ parameters, as well as creating a user interface for the program to make it accessible to others. The program can then be used to determine optical constants of materials, taking into account oxidation gradients of the material. The program can conceivably take into account roughness as well, by approximating the surface roughness with a multilayer varying from the $n$ of air to the $n$ of the material. For details on other ways to take roughness into account, see Niki Farnsworth Brimhall's thesis [12].

# Appendix A

# The Code

## A.1  Data fitting in Matlab

This is the actual program that fits the reflectance data to determine the optical

constants $\delta$ and $\beta$. It uses an unconstrained method (fminunc) to minimize the

squared difference between the calculated and measured data. Give the program a

range, and it will choose the best few starting points and proceed to fit the data and

determine optical constants. It will also graph the function $s$ we want to minimize.

The program is made up of three separate m files.

### A.1.1  Datafitting_8.m

This is the main function that the user runs the program from. It calls the other two

files when necessary.

```
%Fitting program that chooses the best initial guess for you.
%Begins with array of equally spaced initial guesses and chooses
%the 3 with the lowest s.
%Uses FMINUNC only after choosing 3 initial guesses.
%Fits only n2. Fixes substrate and air.
%n1, n2, n3 are hard coded.
%Plots surface that we minimize s with respect to d and b
```

```matlab
%Inputs computed R with added error.

clear; close all;

n2=0.854+0.052*i; theta=1:50;
R=funcfit_7(n2,theta)+normrnd(0,0.0001,1,length(theta));

%Choose a range for the program to find an initial guess
delta=.1:.01:.2; beta=.03:.01:.07; stepd=length(delta);
stepb=length(beta);

%Let it choose it's own initial guess by looping through deltas
%and betas and choose the combination with the lowest s

for d=1:stepd; %delta loop.
    for b=1:stepb; %beta loop

        %Now we minimze the leastsq function
        s=leastsq_7([delta(d),beta(b)],theta,R);

        %This is where the program organizes the initial guesses
        %for later sorting
        index=b+(d-1)*stepb;
        ss(index)=leastsq_7([delta(d),beta(b)],theta,R);

        S(d,b)=leastsq_7([delta(d),beta(b)],theta,R);
        %d and b in the loop index need to be integers to work
    end
end

%This is where the program picks out the 3 best initial guesses
[r,idx]=sort(ss) for mndx=1:3
    bb(mndx)=mod(idx(mndx),3);
    if (b==0)
        b=3;
    end
    dd(mndx)=(idx(mndx)-b)/stepb+1;
end

%Now fit the data with fminunc
%Continue fitting until we reach an accuracy of 1e-5
option=optimset('TolX',1e-4);
[a1,fval,exitflag,output,grad,hessian]=fminunc(@leastsq_7,
  [dd(1),bb(1)],option,theta,R)

%This is where we find the error matrix from the output of the fit
sigmasq=fval/(length(theta)-2); sigma_delta=sqrt(hessian(1,1));
sigma_beta=sqrt(hessian(2,2)); error=2*sigmasq*hessian^(-1);
errnorm=[1 error(1,2)/(sigma_delta*sigma_beta);
  error(2,1)/(sigma_delta*sigma_beta) 1]
```

```
n2=1-a1(1)+i*a1(2); %Reconstruct n2 from delta and beta

%Now we plot the final fit with the data
Rplot=funcfit_7(n2,theta); plot(theta,R,'b*',theta,Rplot,'r-')
xlabel('theta') ylabel('R') title('Final fit and Data')

disp('Press any key to continue') pause

%Plot s with respect to delta and beta
surf(beta,delta,log(S)) xlabel('beta *10','FontSize',16)
ylabel('delta *10','FontSize',16) zlabel('log(s)','FontSize',16)
title('Surface plot of s function to minimize','FontSize',16)
```

## A.1.2   leastsq_7.m

This is the function that is minimized. It computes the square of the measured data minus the computed data.

```
function s=leastsq_7(a,theta,R)

n2=1-a(1)+i*a(2); %Reconstruct n from delta and beta
d=R-funcfit_7(n2,theta); s=d*d';
```

## A.1.3   funcfit_7.m

This is the function that computes the expected reflectance and transmission based on input optical constants. This function is called by both Datafitting_8.m and leastsq_7.m.

```
function Rtot=funcfit_7(n2,theta)

n1=1; n3=0.9+0.5*i;

n=[n1;n2;n3];
%calculate the reflectance and transmission of a multilayer stack
x=[0;10;0]; %Thicknesses in nanometers
fractionp=0.5; %fraction of p polarized light
fractions=1-fractionp; %fraction of s polarized light
lambda=60; %wavelength in nm
k=2*pi*n/lambda; angles=length(theta); layers=length(n);
```

```
surfs=layers-1;
%Create a matrix with k duplicated in every column
km=k(:,ones(1,angles)); ky=k(1)*cosd(theta);
kym=ky(ones(layers,1),:);
%Create a matrix with ky duplicated in every row
%Matrix with all possible combinations of k and ky combined
kz=sqrt(km.^2-kym.^2); kzs=circshift(kz,-1);
%Shift kz by one to compute fresnel coefficients
kz=kz(1:surfs,:); kzs=kzs(1:surfs,:); xm=x(:,ones(1,angles));
xms=circshift(xm,-1); xm=xm(1:surfs,:); xms=xms(1:surfs,:);
nm=n(:,ones(1,angles)); nms=circshift(nm,-1); nm=nm(1:surfs,:);
nms=nms(1:surfs,:);

%Now compute the Fresnel coefficients for s and p polarized light
den1=kzs+kz; den2=kz.*nms.^2+kzs.*nm.^2; Fs21=(kzs-kz)./den1;
Fs12=-Fs21; Gs12=2*kz./den1; Gs21=2*kzs./den1;
Fp12=(nms.^2.*kz-nm.^2.*kzs)./den2; Fp21=-Fp12;
Gp12=2*nm.*nms.*kz./den2; Gp21=2*nm.*nms.*kzs./den2;
C1=exp(i*kz.*xm./2); C2=exp(i*kzs.*xms./2);
As11=Gs21.*C1.*C2-Fs21.*Fs12.*C1.*C2./Gs12;
As12=Fs12.*C1./(Gs12.*C2); As21=-Fs21.*C2./(Gs12.*C1);
As22=1./(C1.*C2.*Gs12);
Ap11=Gp21.*C1.*C2-Fp21.*Fp12.*C1.*C2./Gp12;
Ap12=Fp12.*C1./(Gp12.*C2); Ap21=-Fp21.*C2./(Gp12.*C1);
Ap22=1./(C1.*C2.*Gp12);

%Now compute the matrix elements and combine the matrices
Cs11=As11(1,:); Cs12=As12(1,:); Cs21=As21(1,:); Cs22=As22(1,:);
Cp11=Ap11(1,:); Cp12=Ap12(1,:); Cp21=Ap21(1,:); Cp22=Ap22(1,:);
for m=2:surfs-1;
    Cs11=Cs11.*As11(m,:)+Cs12.*As21(m,:);
    Cs12=Cs11.*As12(m,:)+Cs12.*As22(m,:);
    Cs21=Cs21.*As11(m,:)+Cs22.*As21(m,:);
    Cs22=Cs21.*As12(m,:)+Cs22.*As22(m,:);
    Cp11=Cp11.*Ap11(m,:)+Cp12.*Ap21(m,:);
    Cp12=Cp11.*Ap12(m,:)+Cp12.*Ap22(m,:);
    Cp21=Cp21.*Ap11(m,:)+Cp22.*Ap21(m,:);
    Cp22=Cp21.*Ap12(m,:)+Cp22.*Ap22(m,:);
end if surfs<1
    Cs12=Cs11.*As12(surfs,:)+Cs12.*As22(surfs,:);
    Cs22=Cs21.*As12(surfs,:)+Cs22.*As22(surfs,:);
    Cp12=Cp11.*Ap12(surfs,:)+Cp12.*Ap22(surfs,:);
    Cp22=Cp21.*Ap12(surfs,:)+Cp22.*Ap22(surfs,:);
end

Rs=Cs12./Cs22; Ts=1./Cs22; Rp=Cp12./Cp22; Tp=1./Cp22;

Ttot=fractionp*real(n(1)*conj(n(layers))*kzs(surfs,:)./...
    (n(layers)*conj(n(1))*kz(1,:))).*abs(Tp).^2+...
    fractions*real(kzs(surfs,:)./kz(1,:)).*abs(Ts).^2;
Rtot=fractionp*abs(Rp).^2+fractions*abs(Rs).^2;
```

# Appendix B

# Instrumentation

For XPS, an SSX-100 ESCA (Electron Spectroscopy for Chemical Analysis) Spectrometer is used to collect the electron binding energies. The analysis program ESCAVB compares the peak areas to determine relative percentages. It is calibrated monthly according to the Au4f line at the biding energy 83.98 eV. The Cu2p line at 75.13 eV and Cu3p line at 932.66 eV are also used for better accuracy. The pressure in the analyzing chamber is maintained at between 1 and 2e-9 torr by pumping up and down from atmosphere in a loading chamber. The detector angle is 35 degrees for all scans except the ones taken using the angle-resolved method where the angle is specified. Scans taken using the depth profiling method are rastered with a spot size of 2 mm$^2$, using a SPECS ion gun system (PU-IQE 12/38).

[4] [13] [14]

# Bibliography

[1] http://www.ca.sandia.gov/news/euvl/ .

[2] L. Yarris, "Breakthrough in X-Ray Microscopy Opens New View Inside Living Cells," (1998).

[3] http://www-cxro.lbl.gov/ .

[4] K. D. Bomben, J. F. Moulder, P. E. Sobol, and W. F. Stickle, *Handbook of X-Ray Photoelectron Spectroscopy* (Physical Electronics, Inc., Eden Prairie, Minnesota, 1995).

[5] J. M. Williams and J. Thomas P. Beebe, "High-resolution algorithm for quantitative elemental depth profiling by angle-resolved x-ray photoelectron spectroscopy," J. Vac. Sci. Technol. **15,** 2122–2133 (1997).

[6] C. R. Brundle, G. Conti, H. Graoui, M. Foad, S. Hung, C. Wang, Y. S. Uritsky, P. Mack, and J. Wolstenholme, "Depth-Resolved Composition and Chemistry of Ultra-Thin Films by Angle-Resolved X-Ray Photoelectron Spectroscopy," Characterization and Metrology for ULSI Technology  pp. 307–313 (2005).

[7] E. Spiller, *Soft X-ray Optics* (SPIE Optical Engineering Press, Bellingham, WA, 1994).

[8] D. J. Griffiths, *Introduction to Electrodynamics*, 3rd ed. (Prentice Hall, Upper Saddle River, NJ, 1999).

[9] J. Peatross and M. Ware, *Physics of Light and Optics* (Brigham Young University, Provo, UT, 2005).

[10] R. S. Turley, private communication (2007).

[11] F. James, *Function Minimization and Error Analysis* (CERN Program Library, Geneva, Switzerland, 1998).

[12] N. Farnsworth, "The Effects of Roughness on the Optical Properties of Thorium," (2004).

[13] Y. F. Chen, "Surface effects on angular distributions in x-ray photoelectron spectroscopy," Surface Science **519,** 115–124 (2002).

[14] Y. A. Uspenskii, J. F. Seely, N. L. Popov, A. V. Vinogradov, Y. P. Pershin, and V. V. Kondratenko, "Efficient method for the determination of extreme-ultraviolet optical constants in reactive materials: application to scandium and titanium," J. Opt. Soc. Am. **21,** 298–305 (2004).

# Index

EUV, 1